ISSN 0742-0463, Journal of Volcanology and Seismology, 2008, Vol. 2, No. 2, pp. 118–134. © Pleiades Publishing, Ltd., 2008.
Original Russian Text © G.A. Sobolev, A.A. Lyubushin, N.A. Zakrzhevskaya, 2008, published in Vulkanologiya i Seismologiya, 2008, No. 2, pp. 135–152.

Asymmetrical Pulses, the Periodicity and Synchronization of Low Frequency Microseisms

G. A. Sobolev, A. A. Lyubushin, and N. A. Zakrzhevskaya
Institute of Physics of the Earth, Russian Academy of Sciences, Moscow, 123995 Russia
Received May 17, 2007

Abstract—Seismic records of eight IRIS broadband stations were analyzed at distances of 70 to 7160 km from the magnitude 8.3 Hokkaido earthquake of September 25, 2003. The stations situated in the subduction zone recorded asymmetrical microseismic pulses lasting 3–10 min a few days before the earthquake. No such pulses were observed in the records of the stations situated outside the subduction zone. Similar pulses were also recorded before the magnitude 7.8 Kronotskii, Kamchatka earthquake of 1997. The pulses are hypothesized to have been caused by creeping movements. Synchronous oscillations of microseismic noise with periods of 1–3 h were recorded as far as 3000 km from the Hokkaido earthquake a few days before it occurred. The noise coherence measure increased for stations closer to the epicenter. The question of the source of this coherence remains open. These effects belong to the class of those occurring in dissipative metastable systems; parts of the terrestrial lithosphere during the precursory periods of seismic catastrophes seem to be such systems.

DOI: 10.1134/S074204630802005X

INTRODUCTION

The Earth is acted on by many different oscillating fields in a great range of periods. This process involves partial energy transformations. For example, the energy of electromagnetic waves coming to the Earth from outside excites elastic oscillations in the lithosphere as a consequence of the converse piezoelectric and seismoelectric effects as well as other thermodynamic coupling coefficients connecting the two kinds of energy; elastic stresses appear in the Earth as heat comes in because of thermoelastic coupling coefficients, etc. The intensity of external excitation may be small compared with the forces that act in the Earth, but their influence depends on the energy saturation in rocks and cannot be accounted for by linear effects.

Rhythmic synchronization due to external or internal sources has long been discussed in the geophysical literature. Seismicity has been reported to be influenced by solar activity, earth tides, and climatic factors, among other influences [9, 11, 12, 14, 22, 24, 31, 42]. The synchronization of acoustic signals by electromagnetic pulses has been detected in laboratory experiments [27].

The question of what the threshold is of external excitation sufficient for synchronizing a process that is driven by much greater forces remains open. It is clear that an energetically open system that is sensitive to small external excitations must be in a metastable state [13]. As the system approaches instability, the threshold of effective external excitation decreases. However, the Earth is under constant bombardment of noise due to natural and manmade sources. For this reason the threshold of a detectable effective excitation (including trigger mechanisms) seems to have a finite value above the noise level.

A number of studies in seismic noise in the range 10^2–10^3 s have appeared since the late 1990s, after the installation of the global system of broadband seismic stations. Tanimoto et al. [47] explain the appearance of oscillations in the solid earth by air pressure variations. Kobayashi and Nishida [37] put forward an alternative hypothesis, supposing that the oscillations are excited by numerous small earthquakes whose energy is below the sensitivity of seismic stations. It was shown by these and other workers that oscillations with periods of a few minutes can be observed nearly all the time, and also during quiet time intervals (no large earthquakes).

The appearance of hidden periodic oscillations in the general stream of small earthquakes and microseisms identified in [16, 17] also belongs to the class of phenomena we are discussing. The effect can in principle be treated in the framework of self-organized criticality (SOC) [25, 46] where long-range correlation of seismic events (collective behavior) plays an important part.

It has been found [18, 19] that microseisms with periods of a few minutes also contain some individual pulses of both symmetric and asymmetrical shapes, while a certain periodicity may sometimes be apparent in the sequence of time intervals between successive pulses.

The appearances of rhythms is a widespread phenomenon in the evolution of nonequilibrium systems [10]. It is a known fact that chaotic systems show synchronization effects, especially in the region of attractors [43, 44]. Synchronization in systems dynamics

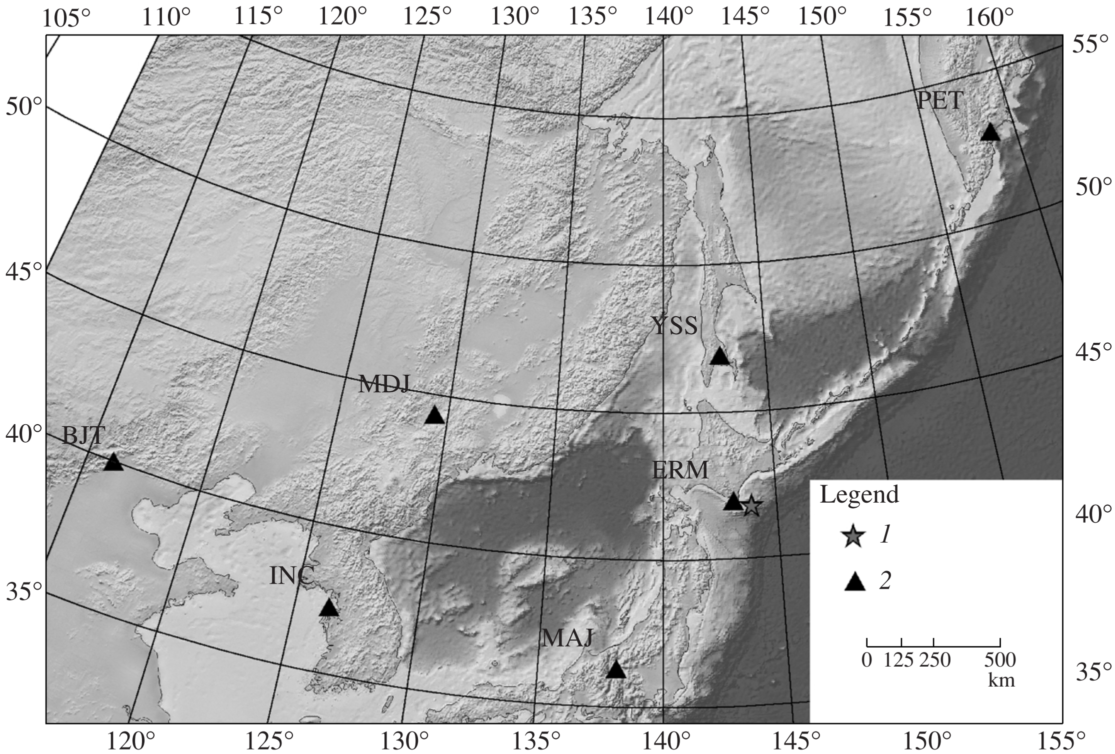

Fig. 1. IRIS seismic stations whose records were used in this study: (*1*) earthquake, (*2*) stations.

may be intermittent, or again, may exhibit stability in some time intervals (with the Lyapunoff exponent negative) [33]. Applications often involve chaotic systems in which the amplitude of oscillation, while remaining finite, chaotically varies over time from minimum to maximum and the attractors are cyclic orbits [15, 45]. Such chaotic systems show phase synchronization [43]. Returning to seismology, phase synchronization of high frequency seismic noise and tides has been noted to have preceded some Kamchatka earthquakes [14].

The exact physical mechanism giving rise to pulses and periodic oscillations with periods of a few minutes in seismology is not yet clear; general theories of catastrophes and phase transitions in energetically open systems need to be specified for inhomogeneous media. The present study treats this problem using seismological observations made before the magnitude 8.3 earthquake of September 25, 2003, off Hokkaido. Considerable attention was paid to synchronization at spatially distant sites on the Earthís surface.

THE DATA

The seismic records examined here were generously provided by the RAS Geophysical Service. They were made at IRIS broadband stations at a sampling rate of 20 Hz: PET, YSS, OBN (Russia), ERM and MAJ (Japan), INC (Korea), MDJ and BJT (China). The amplitude response functions maintain a constant sensitivity for displacement velocity of the instrument base in the range of periods 0.3 to 357 s [21]. In spite of the falloff at longer periods, oscillations can be reliably recorded as long as the 12 and 24-h earth tide peaks. A typical spectrum can be found in [18].

The station positions (except for OBN) are shown in Fig. 1; the OBN station (Obninsk) is in European Russia northeast of Moscow. The September 25 Hokkaido earthquake occurred at 19 h 50 min GT and the epicenter was at 41.81° N, 143.91° E. The stations were thus at different distances from the epicenter between 70 and 7160 km in different seismogeologic settings.

ASYMMETRICAL PULSES

The raw records were averaged over 20 data points, i.e., converted to one sample per second; later the Gaussian trend was calculated [9, 19] with an averaging radius of 100 s to suppress oscillations with periods of a few seconds due to oceanic microseisms and earthquakes.

The records of two of the seven stations examined contained high pulses with amplitudes greater than the 24-h and 12-h tidal oscillations. This phenomenon is shown in Fig. 2, where four-day records made from September 16 to 19, 2003 (days 259 to 262) are displayed: the ERM data was recorded at the Erimo station in southeastern Hokkaido in the subduction zone, nearly in the epicentral zone of the earthquake in question; PET denotes the Petropavlovsk station on the

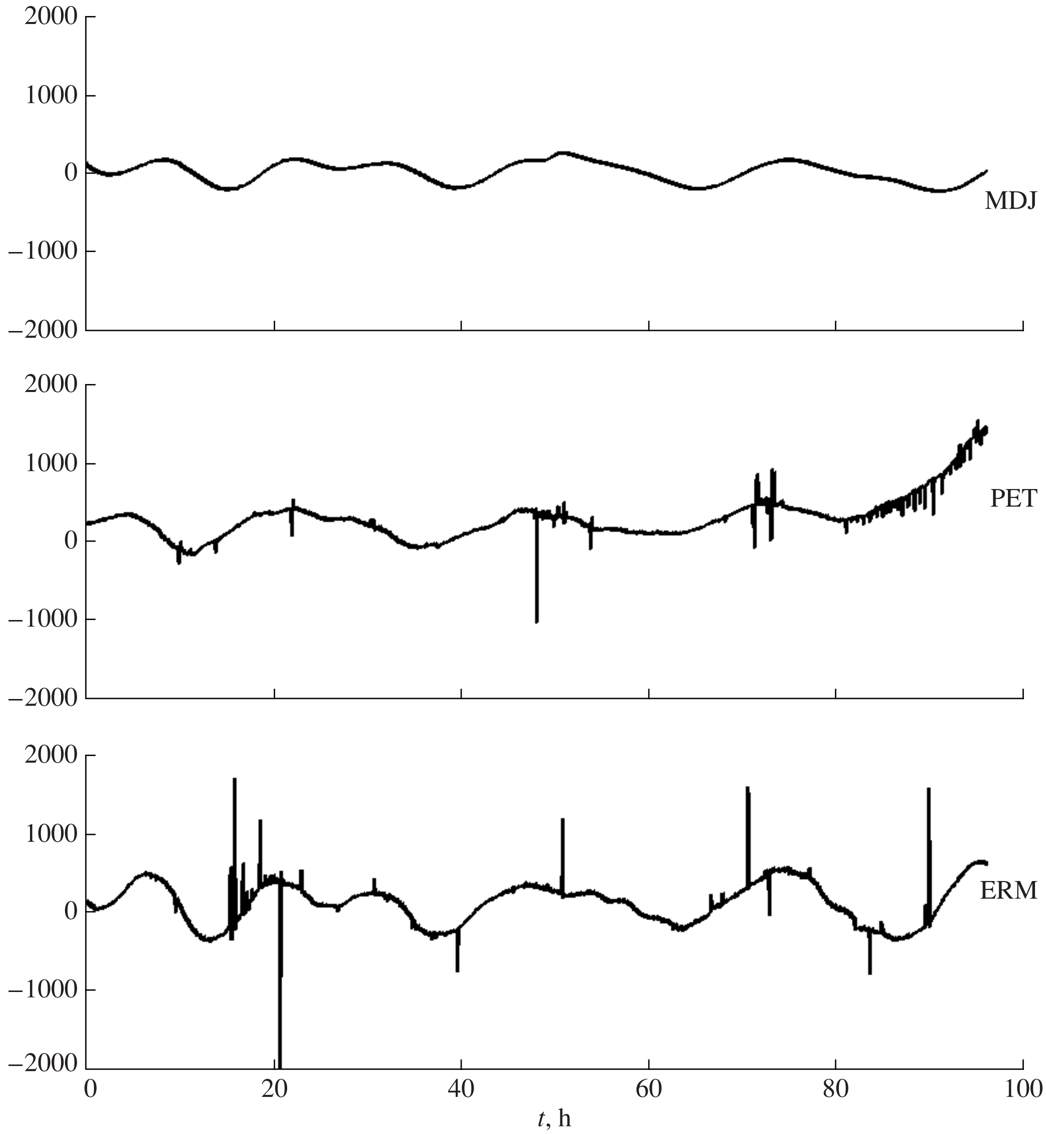

Fig. 2. Sample records of the ERM, PET, and MDJ stations made before the Hokkaido earthquake, with microseism noise with periods of a few seconds being removed. The vertical axis shows displacement velocity in arbitrary units.

coast of Kamchatka, also in the subduction zone; the MDL data was recorded at the Mudanjiang station situated in a continent (northeast China). The ERM and PET trace records contain both isolated positive and negative pulses, and sequences of more frequent pulses upon the background of 24-h and 12-h tides. A sequence of positive polarity in ERM was recorded at 16–20 h (day 259), while a negative sequence in the PET data occupies the interval of 82–98 h (day 262). There are three significant facts to be noted: (1) the pulses were only recorded at ERM and PET, which are in the subduction zone; (2) the times of both isolated pulses and sequences of pulses differ between ERM and PET; and (3) the average pulse amplitudes in ERM are greater than those in PET both in absolute value and in relation to the range of tidal variations. All these circumstances taken together suggest that the sources of the pulses are in the subduction zone. Since we do not know the real sensitivity of these stations in the range of minutes and hours, we shall use relative amplitudes here and below, that is, relative to tides or microseisms with periods of a few seconds.

Consider the structure of the pulses in more detail. The ERM and PET trace records contain sequences of pulses in Fig. 3. The sign in ERM has been reversed (compared with Fig. 2) for convenience of comparison. The low-frequency oscillations with periods of a few hours due to earth tides were removed by subtracting the Gaussian trend of the radius 1000 s. Successive pulses follow at intervals of a few thousand seconds. Looking at pulses 1, 2, 3, and 4 in an extended scale, we

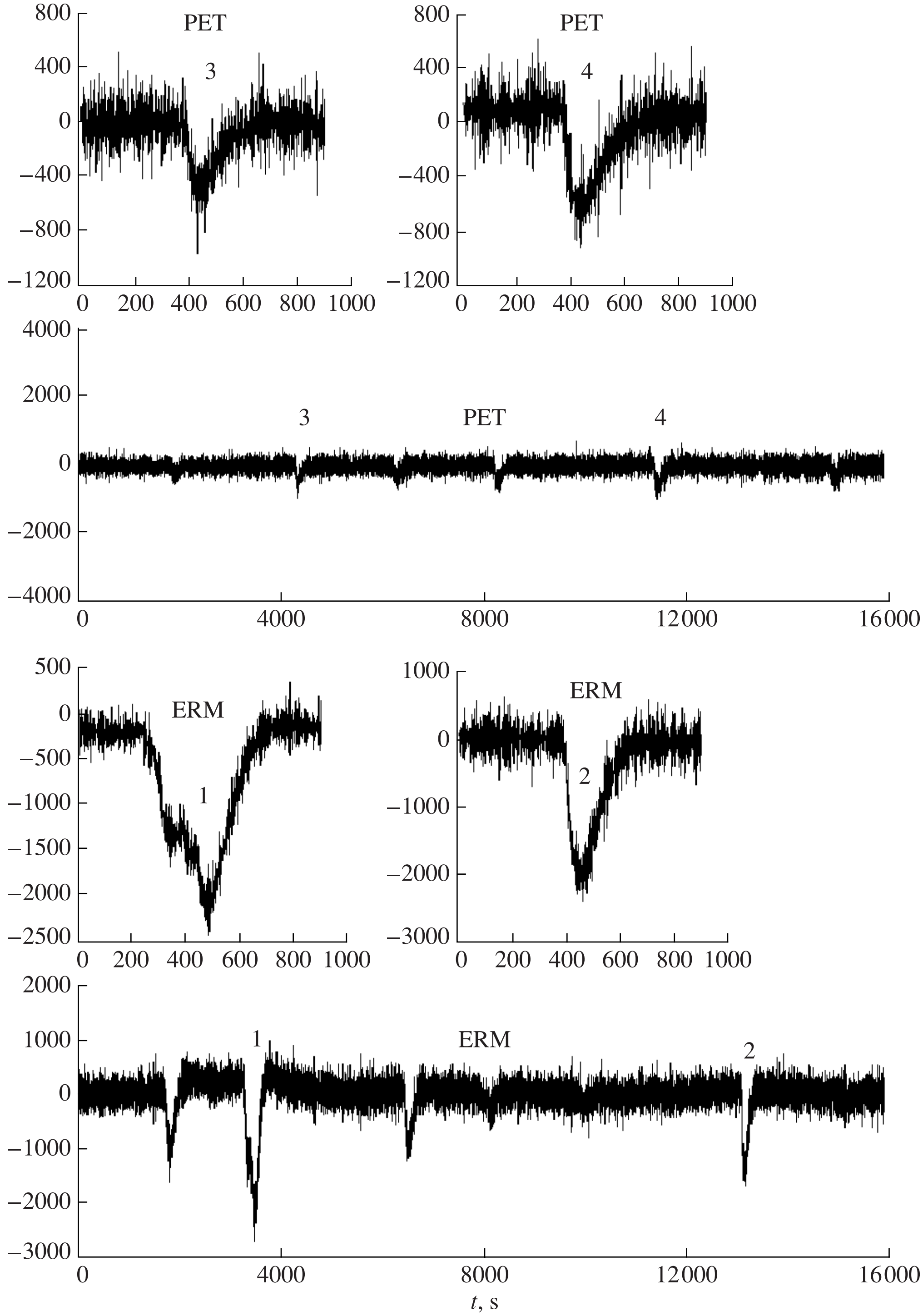

Fig. 3. Some asymmetrical pulses on records of the ERM and PET stations situated in the subduction zone before the Hokkaido earthquake. The vertical axis shows displacement velocity in arbitrary units. For the other explanations see main text.

saw that the rise slopes did not last the same time periods, varying in the range 100–200 s. This range is within the standard frequency range for the IRIS stations [21]. It can be seen (Fig. 3) that the relative pulse amplitudes compared with the high frequency microseism noise at periods of a few seconds are greater at ERM. Since the IRIS channels used here record the vertical velocity component, the pulses under consideration seem to correspond to a unidirectional vertical step in the instrument base motion. Comparison with the horizontal records showed that the amplitudes of the N–S and E–W pulse components are nearly an order below the vertical values, and are comparable with the high-frequency noise amplitudes.

Figure 2 may create the impression that isolated pulses tend to occur around tidal peaks or troughs. Our analysis of the 25-day interval between September 1 and 25, 2003, showed that no significant correlation exists between pulse times and tidal peaks or troughs. The pulse sequences do not coincide either with intervals of distorted tidal oscillations or with periods of weather-induced intensive high frequency noise. This is illustrated by Fig. 4 (PET station). Plot 1 shows the response of the seismic instrument to tidal oscillations. The theoretical vertical displacement component for the tidal wave [49] is shown in plot 2; unfortunately, no strainmeter or tiltmeter tidal observations are available near PET.

A.A. Lyubushin has developed special software [19] for identifying high-amplitude low-frequency pulses (plots 3 and 4). This software performs the following successive steps: applying an average of 20 to the signal; elimination of the low frequency Gaussian trend using the scale parameter (averaging radius) equal to 1000 samples (seconds) to suppress tide-generated motion; and computation of the Gaussian trend using a parameter of 100 s to suppress oscillations with periods of a few seconds due to oceanic microseisms and earthquakes.

The detrending operation was carried out as follows. Let $X(t)$ be an arbitrary finite integrable signal in continuous time. We shall use the phrase ìkernel averaging with scale parameter $H > 0$ to denote the average value $\bar{X}(t|H)$ at time t as given by

$$\bar{X}(t|H) = \int_{-\infty}^{+\infty} X(t+H\xi)\psi(\xi)d\xi / \int_{-\infty}^{+\infty} \psi(\xi)d\xi, \qquad (1)$$

where $\psi(\xi)$ is an arbitrary nonnegative finite symmetrical integrable function, termed the averaging kernel [34]. If $\psi(\xi) = \exp(-\xi^2)$, the quantity $\bar{X}(t|H)$ is called the Gaussian trend with the averaging parameter (radius) H [9, 19].

The above operations will give a signal at intervals of 1 s, whose power spectrum lies in the range of periods approximately between 200 and 2000 s. The same result could be obtained by using ordinary bandpass Fourier filtering, but Gaussian trends are preferable, because they do not generate side-effects due to filter slope; as well, it is then easier to overcome end-point effects due to the finiteness of the sample.

The resulting signal was analyzed by our program to identify high amplitude pulses. To do this, we used the Haar wavelet expansion [30, 38], namely, after application of the direct Haar wavelet transformation we retained a small fraction $(1 - \alpha)$ of wavelet coefficients that were greatest in absolute value, setting $\alpha = 0.9995$. The next step was to perform the inverse wavelet transformation, yielding a sequence of pulses of sufficiently great amplitude with intervals of constant values (previously filled with noise) in between. The operation just described is known in wavelet analysis [30, 38] as denoising. The choice of the Haar wavelet for this operation was suggested by the simplicity of subsequent automatic identification of rectangular pulses. The compression level α controls the number of identifiable pulses and the degree of noise suppression.

Positive pulses (plot 3) appeared in the later half of the interval under study, and were distributed fairly uniformly over time. The negative pulses were much more numerous, while the sequences of frequent pulses mentioned above were observed both in the interval of intensive 12-h tidal oscillations and in the interval of mostly 24-h oscillations. The sequences occurred upon the background of undisturbed high frequency oscillations (plot 5). This plot was obtained by removing the low frequency trend, with the signals with periods between 2 and 16 s being left untouched. This shows that no storm microseisms coming from the nearest water bodies were present at the time [23].

Plot 1 (Fig. 4) shows an anomalous increase in the PET seismic response to tides during the last 5 days before the earthquake. No anomalies in tidal response have been found at the other stations referred to above (except ERM). This last station, which was situated in the subduction zone, ceased operation due to an unknown cause following several failures. According to Prof. M. Kasahara, Hokkaido University, the signal from the automatic ERM station had been available until the time of the earthquake, and the reason that nothing was recorded during this period is unknown.

PERIODICITY OF OSCILLATIONS

It was found in our previous work [17, 18] that the Kronotskii, Kamchatka earthquake was preceded by oscillations with periods of a few tens of minutes on records of some stations. The oscillations appeared with delays of a few hours, both after large teleseismic events and after large foreshocks of the earthquake just referred to. We shall examine the records prior to the Hokkaido earthquake.

We analyzed the periodic structure of microseismic oscillations by considering sequences of times of increase in the seismic amplitude above a specified level. These time series were processed in moving time windows. An orthogonal polynomial of degree 3 was used to remove the low-frequency trend within a window. After detrending we computed a threshold for the window, equal to the product of the absolute median deviation (the median of deviations from the median) and a multiplier (the method parameter) that was usually varied between 1 and 4. The parameter depends on the spike amplitude in the signal and is adjusted experimentally. The next step was to examine the sequence of times of local peaks in the record above the thresh-

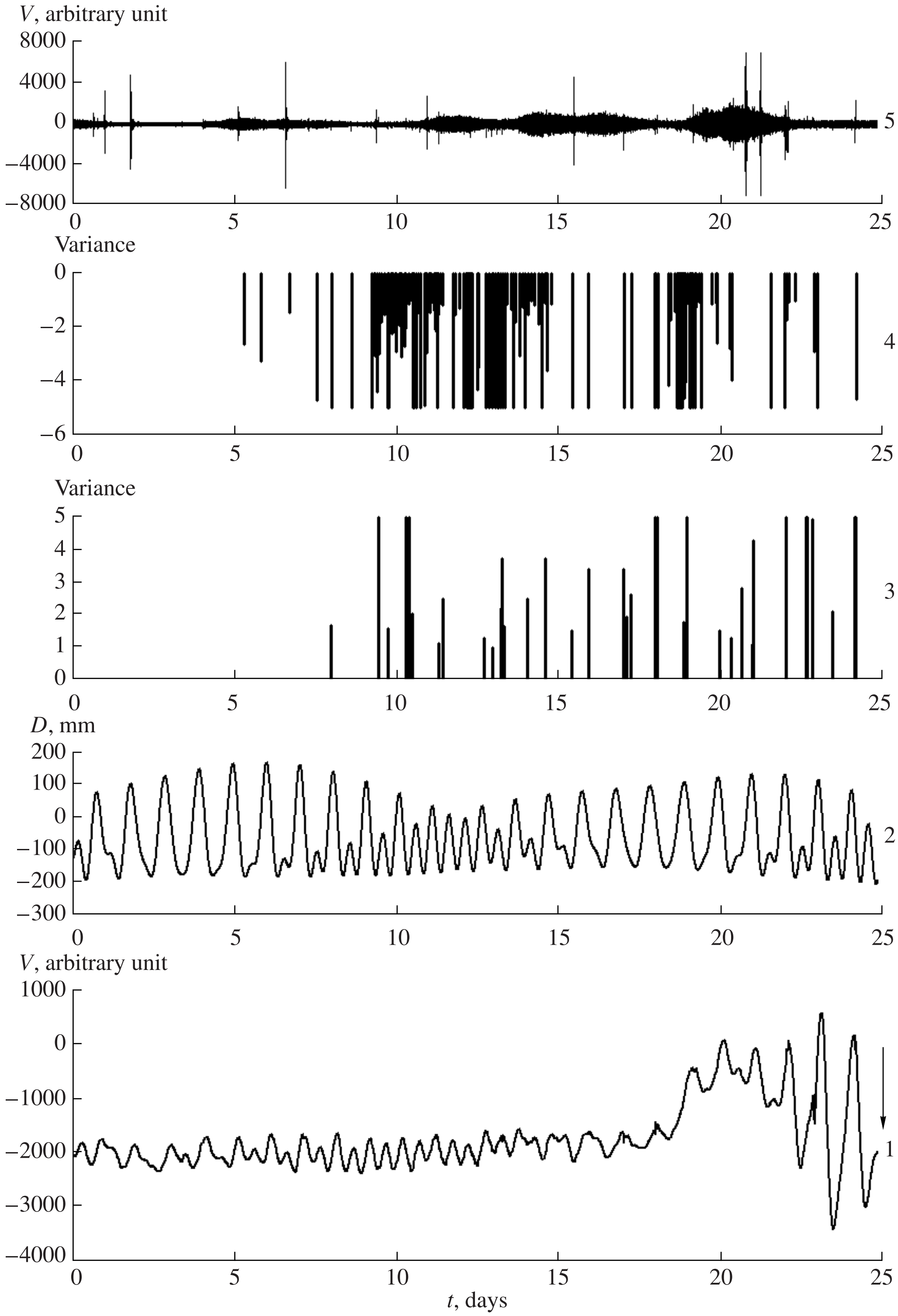

Fig. 4. Comparison of the low frequency component at PET (1) with the theoretical tide for the site of that station (2), times of occurrence of asymmetrical positive (3) and negative (4) pulses and with the level of microseism noise with periods of a few seconds (5). The arrow indicates the Hokkaido earthquake occurrence time.

old. The original time series were thus reduced to a point process consisting of a sequence of times. The times are similar to the sequence of events in an earthquake catalog.

The method used here to detect periodic components in a sequence of events was described in [1]. We considered a model for the rate of events (in the case under consideration for times of significant local maxima, that is, spikes in the microseism time series) that was supposed to contain a harmonic component:

$$\lambda(t) = \mu(1 + a\cos(\omega t + \varphi)), \quad (2)$$

where the frequency ω, the amplitude a, $0 \le a \le 1$, the phase angle φ, $\varphi \in [0, 2\pi]$ and the multiplier $\mu \ge 0$ (which describes the Poisson part of the rate) are model parameters. The Poisson part is thus modulated by a harmonic oscillation.

The increment of the log likelihood of a point process [28] resulting from consideration of a richer (compared with the random stream of events) intensity model with the harmonic component of a specified frequency ω is [1]

$$\Delta \ln L(a, \varphi|\omega) = \sum_{t_i} \ln(1 + a\cos(\omega t_i + \varphi)) + N\ln \omega T/[\omega T + a(\sin(\omega T + \varphi) - \sin(\varphi))]. \quad (3)$$

Here, the t_i are the successive times of identified local maxima in the signal within the window, N is their number, and T is the length of the time window. Let

$$R(\omega) = \max_{a, \varphi} \Delta \ln L(a, \varphi|\omega), \quad 0 \le a \le 1, \quad \varphi \in [0, 2\pi]. \quad (4)$$

The function (4) can be treated as a generalized spectrum for a sequence of events [1]. The plot of this function shows by how much a periodic intensity model is "more advantageous" compared with the completely random model. Maxima of (4) highlight the frequencies that are available in the stream of events.

We denote by τ the time of the right end-point for the moving time window of a given length T_W. Actually, (4) is a function of two arguments: $R(\omega, \tau|T_W)$, which can be visualized in the shape of two-dimensional maps or three-dimensional relief on the plane of arguments (ω, τ). This frequency–time diagram can be used to investigate the dynamics of periodic components as they originate and evolve within the stream under investigation [4, 16–18].

We divided the last 7 days prior to the Hokkaido earthquake into two overlapping intervals. The first of these includes 5760 min (days 262–265 of the year 2003, from September 19 to 22, 2003); the second is 5550 min long (days 265–268, from September 22 to 26, 2003) and terminates before the earthquake occurrence time. We note here that the earthquake occurred at 19 h 50 min on September 25 (day 268). The original records made at a sampling rate of 20 Hz were compressed by averaging over 600 points down to a step of 0.5 min. The computations were then performed in moving windows of 720 min at intervals of 30 min. We searched for maxima of $R(\omega)$ in the range of 60 to 240 min.

Figure 5 shows frequency–time diagrams based on data from five stations, with the station names being indicated above the diagrams. The plots are given only for those stations where periodic oscillations were identified. These did not appear at MAJ and OBN, while ERM was not in operation during that period, as mentioned above. Two large teleseismic magnitude 6.6 earthquakes occurred during the second half of that period, with the occurrence times being indicated by arrows. One occurred at 18 h 16 min on September 21 (day 264) at the epicenter 19.72' N, 95.46' E and the other after an interval of 10 h (day 265) at the epicenter 21.16'N, 71.67' W. Oscillations of periods 160–180 min arrived after a delay of about 400 min and lasted about 600 min.

The next greatest burst of periodic oscillations occurred September 25 (day 268) 16 h before the Hokkaido earthquake; this is shown in the frequency–time diagrams of Fig. 6 (the interval 4300 to 5100 min). The oscillations were only observed at three stations (PET, YSS, and MDL), and also had periods of about 120 min, in addition to those mentioned above. No large ($M > 5$) earthquakes preceded these oscillations. The common feature in the periodic oscillations recorded during the last 5 days before the Hokkaido earthquake consists in the fact that they were most noticeable at the stations nearest to the epicenter. The intervals of such periodic oscillations may repeat themselves, as is the case with the 2300–3300 min region in Fig. 6. An analysis of long-term observations (a few months or years) is required to see whether their occurrence before large earthquakes is not accidental, but this is outside the scope of the present study.

SYNCHRONIZATION EFFECTS

One sign that a nonlinear dynamic system is unstable before a catastrophe may consist in synchronization of oscillations, including random noise [43]. The lithosphere is just such a system, and it is not ruled out that the stream of microseisms at different points on the Earth's surface is subject to synchronization, especially immediately before a large earthquake. We have investigated the phenomenon of synchronization using two methods.

In the one of these, we estimated the multifractal measure of synchronization [8, 9] or the evolution of the spectral measure of coherent behavior exhibited by variations of the generalized Hurst exponent for different sets of stations. We give a summary of the method, referring the reader to [8, 9] for details.

Let $X(t)$ be a signal. We choose to characterize the variability $\mu(t, \delta)$ of $X(t)$ on the interval $[t, t + \delta)$ by the range:

$$\mu(t, \delta) = \max_{t \le s \le t+\delta} X(s) - \min_{t \le s \le t+\delta} X(s). \quad (5)$$

The Lipschitz–Holder exponent $h(t)$ for a point t is defined as the limit

$$h(t) = \lim_{\delta \to 0} \frac{\ln(\mu(t, \delta))}{\ln(\delta)}, \quad (6)$$

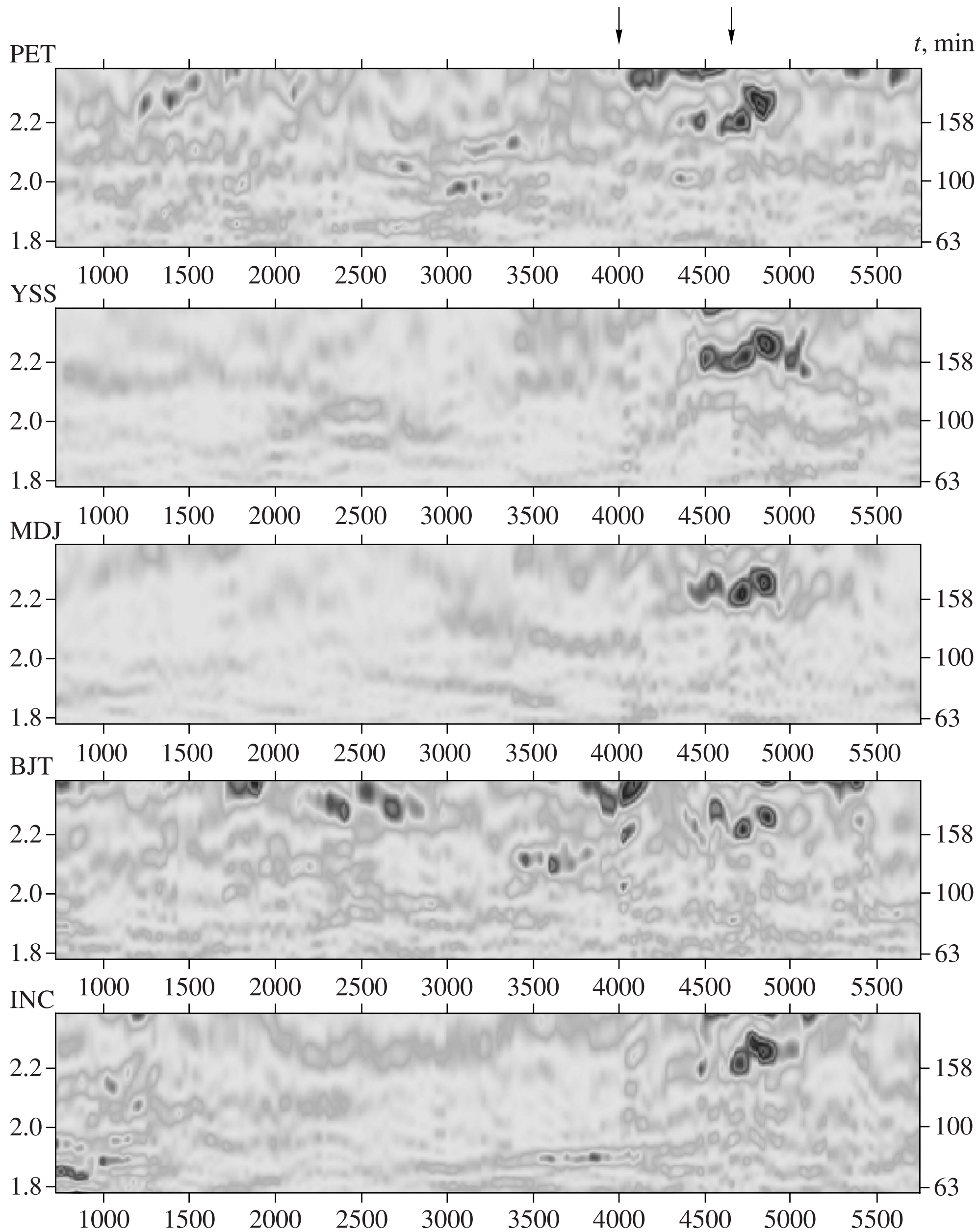

Fig. 5. Frequency–time diagrams of PET, YSS, MDJ, BJT, and INC stations in the interval 7–4 days before the Hokkaido earthquake. The vertical axis shows the period of oscillations in the linear (right) and log (left) scale. The arrows mark the time of teleseismic magnitude 6.6 earthquakes.

that is, the variability measure $\mu(t, \delta)$ decays according to $\delta^{h(t)}$ as $\delta \longrightarrow 0$ in a neighborhood of t.

The singularity spectrum $F(\alpha)$ is defined [32, 40] as the fractal dimension of the set of t for which $h(t) = \alpha$ (i.e., those with the same Lipschitz–Holder index).

A singularity spectrum does not exist for all signals, but only for the so-called scale-invariant ones. Supposing $X(t)$ to be a random process, we now find the mean of the $\mu(t, \delta)$ raised to the power of q:

$$M(\delta, q) = M\{(\mu(t, \delta))^q\}. \tag{7}$$

A random process is scale-invariant, when $M(\delta, q)$ decays according to $\delta^{\kappa(q)}$ as $\delta \longrightarrow 0$ 0, that is, when the following limit exists:

$$\kappa(q) = \lim_{\delta \to 0} \frac{\ln M(\delta, q)}{\ln(\delta)}. \tag{8}$$

If $\kappa(q)$ is a linear function: $\kappa(q) = Hq$, where H = constant and $0 < H < 1$, then the process is a monofractal one. Taking the particular case of Brownian motion, we have $H = 0.5$. The process $X(t)$ is monofractal if $\kappa(q)$ is nonlinear.

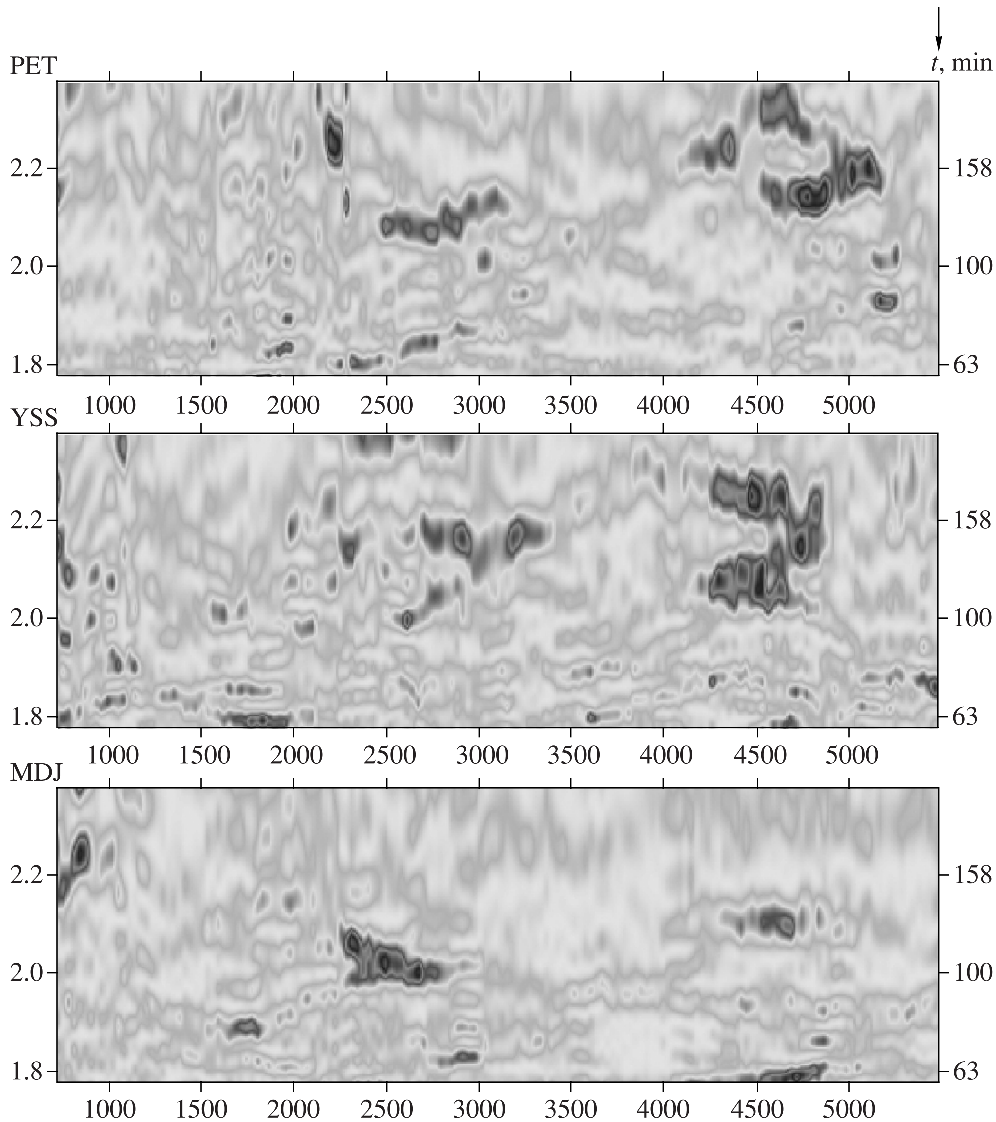

Fig. 6. Frequency–time diagrams of PET, YSS, and MDJ stations for the last four days before the Hokkaido earthquake. The vertical axis shows the period of oscillations in the linear (right) and log (left) scale. The arrow marks the time of the Hokkaido earthquake.

The purpose of raising q to different powers in (7) is to ascribe different weights to time intervals with large and small variability measures. When $q > 0$, the main contribution to the mean $M(\delta, q)$ is due to time intervals with large variability, while those with small variability contribute the most when $q < 0$.

When the spectrum $F(\alpha)$ is estimated in moving time windows, its evolution can provide information on the variation of structure in the chaotic pulsations of a time series. In particular, the position and width of the support of $F(\alpha)$ (the values of α_{min}, α_{max}, $\Delta\alpha = \alpha_{max} - \alpha_{min}$ and α^*, the last being the value at which $F(\alpha)$ is the greatest: $F(\alpha^*) = \max_{\alpha} F(\alpha)$), are characteristics of the noise. The quantity α^* may be called a generalized Hurst exponent. For a monofractal signal the value of $\Delta\alpha$ must be zero, and $\alpha^* = H$. As to the value of $F(\alpha^*)$, it is equal to the fractal dimension of those points for whose neighborhoods the scaling relation (8) holds.

Below we calculate the singularity spectrum $F(\alpha)$ using the method of fluctuation analysis after removing the scale-dependent trends [36] using the software set described in detail in [8, 9].

One commonly has $F(\alpha^*) = 1$, but there are windows for which $F(\alpha^*) < 1$. We recall that in the general case (not for time series analysis alone) the quantity $F(\alpha^*)$ is equal to the fractal dimension of the support of the multifractal measure [32].

We note that the analysis of variations in the multifractal properties of time series resulting from geophysical monitoring observations is a promising trend in the data analysis for solid Earth physics [8, 9, 29, 48], since multifractal analysis is capable of investigating signals that, viewed from covariance and spectral theory, are nothing more than white noise or Brownian motion.

The analysis is done in order to detect the effects of coherent (synchronous) behavior of microseisms with periods of a few minutes after converting the raw data to the associated singularity spectra estimated in moving time windows. Below we characterize the singularity spectra by values of α^* at which the spectrum is the greatest. The values of α^* characterize the most typical singularity, which is most frequently encountered within a moving window when the noise component of microseisms exhibits a self-similar behavior. Prior to this processing, we converted the data to 30-s time intervals by averaging and by decimating the raw seismograms by a factor of 600 that were recorded at a rate of 20 Hz.

Time series showing the evolution of α^* were obtained by using a moving window of 1440 30-s data points, that is, 12 h, with any two adjacent windows being at a distance of 120 points or 1 h. Polynomials of degree 4 were used to remove scale-dependent trends [8, 9].

The subsequent analysis was performed in order to detect coherent variations in α^*. Coherent elements of behavior that could have a phase shift and be observed at several stations simultaneously were identified by estimating canonical coherences in moving time windows as developed by Lyubushin [2] to search for earthquake precursors in data supplied by low frequency geophysical monitoring. The analysis to be given below essentially follows the technique used in [8] to investigate variations in the generalized Hurst constant. Lyubushin et al. [5, 7] applied this method to the analysis of multivariate hydrologic and oceanographic time series. Sobolev and Lyubushin [20] used this spectral measure of coherent behavior to identify synchronous effects in low frequency microseisms recorded at several stations before the December 26, 2004 Sumatra earthquake.

The spectral coherence measure $\lambda(\tau, \omega)$ is constructed as the modulus of the product of component canonical coherences

$$\lambda(\tau, \omega) = \prod_{j=1}^{q} |\nu_j(\tau, \omega)|. \tag{9}$$

Here, q is the total number of time series simultaneously analyzed (the dimension of the associated multivariate time series), ω the frequency, τ the time coordinate of the right end-point of the moving time window consisting of a certain number of adjacent data points, and $\nu_j(\tau, \omega)$ is the canonical coherence of the jth scalar time series, which describes the strength of coupling between this series and the other series.

The quantity $|\nu_j(\tau, \omega)|^2$ is an extension of the usual quadratic coherence spectrum between two signals to the case of a vectorial, not scalar, second signal. The inequality $0 \le |\nu_j(\tau, \omega)| \le 1$ holds and, the closer the value of $|\nu_j(\tau, \omega)|$ to unity, the stronger is the linear coupling connecting the variations at a frequency ω in the time window having the coordinate τ of the jth series to similar variations in all the other series. Accordingly, the quantity $0 \le \lambda(\tau, \omega) \le 1$ describes (by construction) the effect of the combined coherent (synchronous, collective) behavior of all the signals. We note that, by construction, the values of $\lambda(\tau, \omega))$ belong to the interval [0,1] and, the closer a value is to unity, the stronger is the coupling between variations of components of the multivariate time series $Z(t)$ at a frequency ω for a time window with the coordinate τ. It should be stressed that absolute values of $\lambda(\tau, \omega))$ can only be compared for the same number (q) of simultaneously processed time series, because λ decreases as a product of q quantities, all below unity, as shown by (9).

Implementation of this algorithm requires an estimate of the spectral matrix for the original multivariate series available in each time window. We have chosen to use a third-order vectorial autoregressive model [41]. The function $\lambda(\tau, \omega))$ was obtained using a time window of 109 values as the length of the time window. Since each value of α^* was based on a time window of 12 h, and the windows were moved at intervals of 1 h, the length of the time series for estimating the spectral matrix is $(109 - 1) \cdot 1 + 12 = 120$ h = 5 days. All the technical details for calculating (9) can be found in [2, 9].

The results of the foregoing analysis are as follows. The largest set involved in the calculation consisted of six stations, namely, YSS, MDJ, INC, BJT, PET, and OBN. The records of ERM and MAJ were not used, because the first of these (see above) did not record microseisms during the final period (days 265 to 268), while the second was not in operation between days 251 and 258. It was found (Fig. 7) that synchronization, as derived from records of the six stations, was seen two days before the earthquake (the interval from 33000 to 35000 min). The synchronization involved periods of 3 h (frequency 0.005 1/min) and longer. As the number of stations decreased, the amplitude of $\lambda(\tau, \omega))$ increased in accordance with (9). One significant circumstance consisted in the fact that, when all combinations of three stations were tried, the effect was the most pronounced for those closest to the Hokkaido earthquake epicenter. The frequency–time diagram for these stations (YSS, MDJ, and INC) is shown in Fig. 8.Three features are to be noted: (a) synchronization with period ~3 h (frequency ~0.005 1/min) began 9 days before the earthquake (23000 min); (b) synchronization failed in the interval 29000 to 31 000 min, followed by subsequent recovery; (c) the synchronization was the most pronounced and in a wide range of periods two days before the earthquake (33000 to 35000 min). The

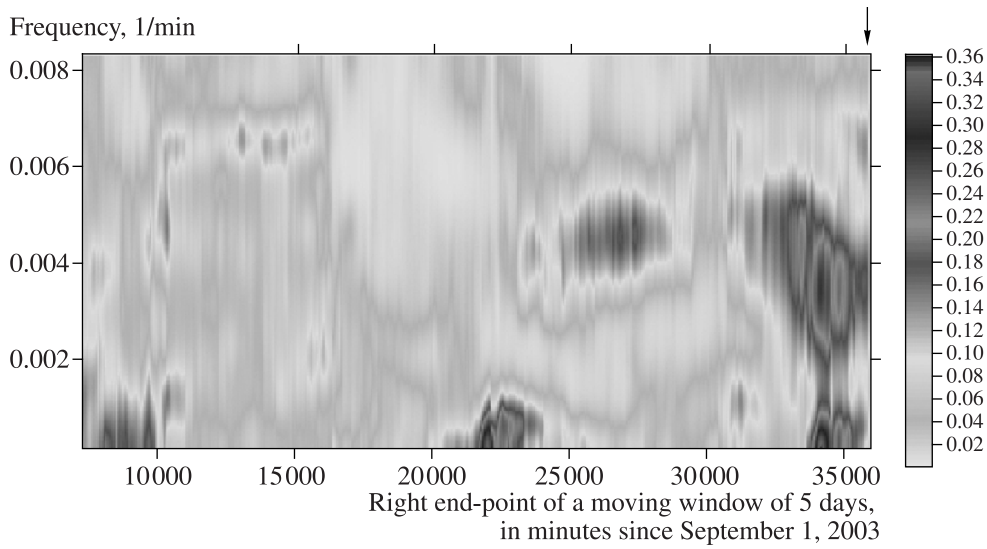

Fig. 7. The evolution of the spectral measure of coherent behavior for variations in the generalized Hurst exponent estimated in moving time windows of 12 h at intervals of 1 h for six stations: OBN, PET, BJT, INC, YSS, and MDJ. The arrow marks the time of the Hokkaido earthquake.

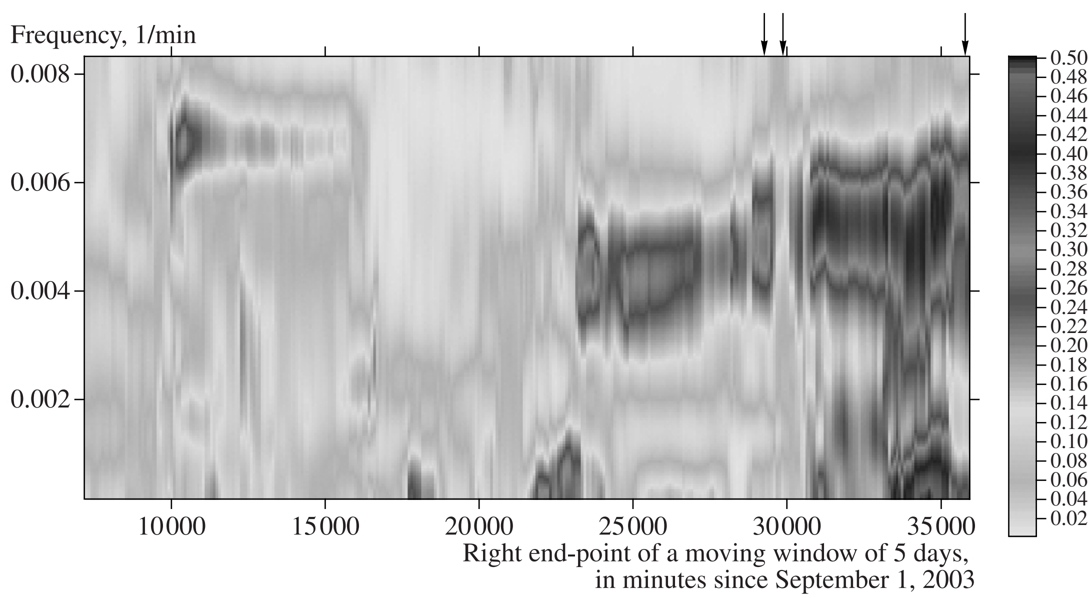

Fig. 8. The evolution of the spectral measure of coherent behavior for variations in the generalized Hurst exponent estimated in moving time windows of 12 h at intervals of 1 h for three stations: YSS, MDJ, and INC. The arrow marks the time of the Hokkaido earthquake.

interval of failed synchronization was identical with the time of occurrence of the large earthquakes indicated above; this is naturally explained by the different arrival times of the seismic waves at the stations.

We note that there is an analogue of (9) which involves, not the canonical coherences, but the canonical correlations between wavelet coefficients at different levels of detail available in the orthogonal expansions of the original signals in a moving time window. One thus obtains a wavelet measure of synchronous behavior pertinent to the components of a multivariate time series [3, 6, 9]. Sobolev and Lyubushin [20] used both of these measures, i.e., the spectral and the wavelet ones, in order to detect synchronization effects.

The previous method for detecting synchronization effects was to convert raw 30-s data to time series of the generalized Hurst constant for singularity spectra estimated in moving time windows. It is also advisable to attempt to use values of the ordinary Hurst constants for the same purpose.

We recall that the ordinary Hurst constant H [32, 35, 39] for a time series is estimated as the slope in a linear regression between $\ln(RS(s))$ and $\ln(s)$. Here, s is the length of the time interval, $RS(s)$ is the mean ratio of the range (the difference between the greatest and least values) of accumulated sum of deviations from the sample mean to the sampling estimate of the standard deviation on all time intervals of length s. The value of $RS(s)$ is calculated by averaging over all intervals of this length that are accommodated by the available time series sample, that is, one has $RS(s) \sim s^H$. For a self-similar time series $Z(t)$ whose power spectrum $S_{ZZ}(\omega)$ behaves according to the power law $S_{ZZ}(\omega) \sim \omega^{-\alpha}$ as $\omega \longrightarrow 0$, one has $\alpha = 2H + 1$, the value of $RS(s)$ being calculated for the increments $x(t) = Z(t + 1) - Z(t)$.

The relation $S_{ZZ}(\omega) \sim \omega^{-\alpha}$ is commonly used for a popular and rapid method of estimation of the Hurst constant $H = (\alpha - 1)/2$ through the slope α of the power spectrum in a log–log plot, that is, as the slope in a linear regression $\ln(S_{ZZ}(\omega))$ and $-\ln(\omega)$. If we try to use this method to estimate the variation of the Hurst constant in moving time windows, we have to estimate the spectral exponent α from short samples. However, estimates of power spectra are subject to statistical fluctuations (because of the shortness of the sample), which are also reflected in estimates of α.

An alternative method for calculating the spectral exponent α is to make use of the orthogonal wavelet expansion of signal fragments in a current time window. The Hurst constant can be estimated from the rate of growth of the mean squared absolute values of wavelet coefficients [38]:

$$W_k = \sum_{j=1}^{N^{(k)}} \left|c_j^{(k)}\right|^2 / N^{(k)}. \tag{10}$$

Here, the $c_j^{(k)}$ are coefficients of the orthogonal discrete wavelet expansion of a sample of a self-similar time series, $k = 1, \ldots, m$ is the number of the level of detail available in the expansion, and $N^{(k)}$ is the number of wavelet coefficients at the level of detail k, $N^{(k)} \le 2^{(m-k)}$. In that case, similarly to the relation for the rate of growth of a power spectrum, we have $W_k \sim (s_k)^{2H+1}$, where s_k is the typical time scale of the level of detail k. Since $s_k = 2^k–2^{(k+1)}$, it follows that

$$\log_2(W_k) \sim k^{(2H+1)}. \tag{11}$$

It thus appears that the slope of the least-squares line based on $(\log_2(W_k), k)$ pairs gives an estimate for $2H + 1$. This method of estimating the Hurst constant is less subject to statistical fluctuations than that in terms of the spectral exponent because of the relatively short sample length within the moving window, by virtue of the averaging (10).

For the data under consideration, the following simple measure of synchronous behavior based on the estimate of the Hurst constant from (11) has turned out to be unexpectedly efficient. After passage to 30-s time intervals, the Hurst parameter H was estimated in moving time windows 2880 values long (1 day) at intervals of 120 values (1 h). In order to exclude the influence of tidal variations, we removed a polynomial trend of degree 8 in each window and calculated the wavelet power spectrum (10) based on the residuals. We chose to use the optimal orthogonal Daubechies wavelet, with the number of moments set equal to zero being 2 to 10; the wavelet realizes the minimum entropy for the distribution of squared wavelet coefficients [38] for the first 8 levels of detail in the wavelet expansion (scales or "periods" between 1 and 256 min at intervals of 0.5 min).

We denote the estimate of the Hurst parameter for the kth time series as a function of τ by $H_k(\tau)$, which is the time coordinate of the right end-point of the time window. The detrended values of $H_k(\tau)$ based on the residuals assumed both negative and positive values. We then take those time windows for which these estimates are positive. The special interest in the positive estimates is related to the fact that the Hurst constant for a self-similar process must lie between 0 and 1 [32, 39]. For this reason the inequality $H_k(\tau) > 0$ provides indirect evidence for fractal self-similar behavior of the low frequency seismic noise. Consequently, it is of interest to find such time windows for which the estimates of the Hurst constant are positive for all the processes under simultaneous analysis, since this indicates some low frequency synchronization. Such windows can be found using the measure

$$\chi(\tau) = \prod_k \max(0, H_k(\tau)). \tag{12}$$

The quantity (12) is obviously zero, if the estimate of $H_k(\tau)$) is not positive at least for one signal.

Synchronization based on (12) was apparent from a joint analysis of records made at five stations (YSS, MDJ, INC, BJT, and PET) (Fig. 9a) and their variable combinations of two to four stations. The synchronization failed when the OBN records were included. It appears from Fig. 9a that the variations of H had two maxima two days before the Hokkaido earthquake, around 34000 and 35000 min.

When variants with equal numbers of stations are to be compared, we are justified in comparing absolute values of $\chi(\tau)$ in accordance with (12). Various combinations of three stations have led us to the following conclusions. The best result was achieved with YSS, MDJ, and INC, the value of $\chi(\tau)$ being 0.03 (Fig. 9*b*). It was only the last (before the earthquake) anomaly, around 35000 min, which was well-pronounced. The above three stations are the closest ones to the epicenter. When YSS was replaced with PET, the result was to

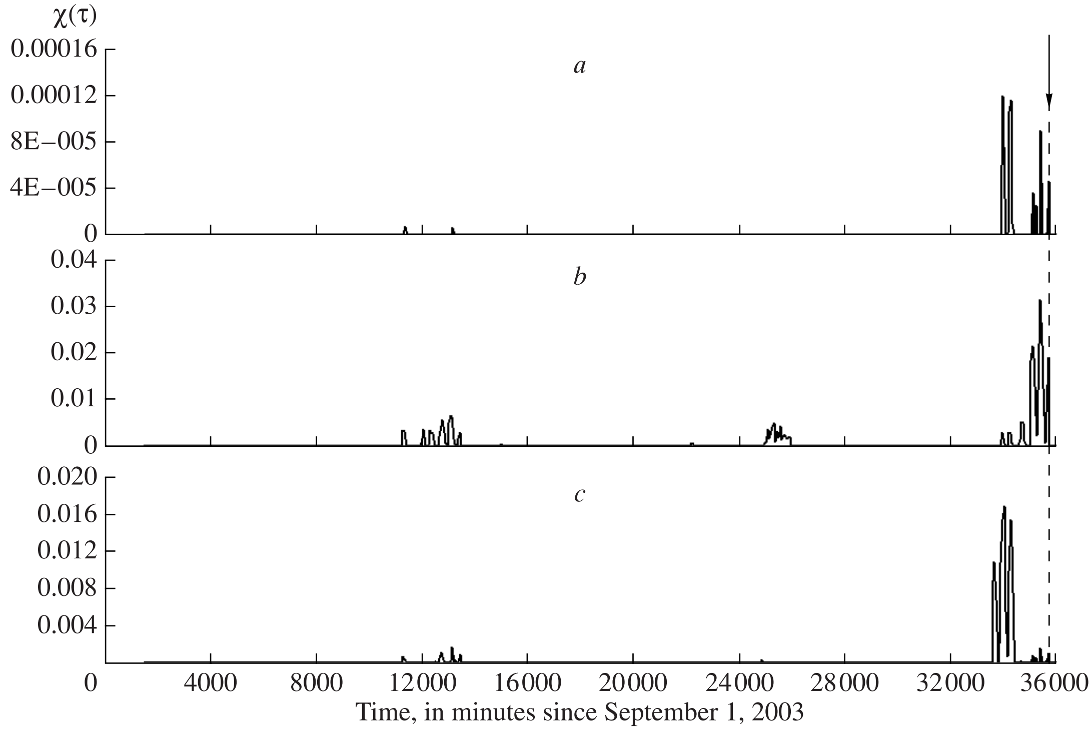

Fig. 9. Estimating the synchronization measure $\chi(\tau)$ (12) in moving windows of 24 h: (*a*) for stations BJT, INC, MDJ, PET, and YSS; (*b*) for stations INC, MDJ, and YSS; (*c*) for stations INC, MDJ, and PET. The arrow marks the time of the Hokkaido earthquake.

diminish the amplitude to 0.018 (Fig. 9*c*), with the best-pronounced anomaly being that around 34000 min.

RESULTS AND DISCUSSION

One outstanding feature of the microseism structure observed before the Hokkaido earthquake was that the records of the ERM station, which is situated in the epicentral zone of a large earthquake (magnitude 8.3), contained pulses lasting 100 to 200 s whose amplitudes were considerably above the level of usual microseisms having periods of a few seconds and above the response of the seismic instrument to earth tides (Figs. 2, 3). One would like to know the extent to which that phenomenon is unique. The answer has to wait for new data, until a seismic station will again happen be near the epicenter of a large earthquake, especially if this should occur in a subduction zone.

What we can do at present is to compare ERM records made in September 2003 (before the Hokkaido earthquake) with records made during a similar interval of time following the termination of the aftershocks in 2006. Figure 10 presents such a comparison for days 259–262 in 2003 (plot 1) and in 2006 (plot 3). No asymmetrical pulses were recorded in 2006. The records of a station far from the subduction zone (MDJ, plots 2 and 4) are also shown. The correlation coefficient between the ERM and MDJ trend components (plots 3 and 4), when recorded during the quiet period, reached 80%, with a corresponding time shift due to the position of the ERM station somewhat to the east. The coefficient was somewhat smaller (76%) during the precursory period of the Hokkaido earthquake (plots 1 and 2).

From this analysis we can draw the following conclusions: (a) the pulses appeared in the subduction zone; (b) their occurrence is not an invariable property of the station installed in the subduction zone; and (c) there is probably a cause-and-effect relationship between the precursory processes of the Hokkaido earthquake and the occurrence of pulses with periods of a few minutes.

It is also advisable to discuss the relationship between the occurrence of frequent and similar-shaped asymmetrical pulses and the precursory processes of large earthquakes. We are in a position to do so based on data recorded at the same station (PET) before two earthquakes. Figure 2 (plot PET) presents an example of such a sequence six days before the Hokkaido earthquake in the interval 82 to 98 h. We remind the reader that Sobolev et al. [18] described the occurrence of a sequence of unidirectional pulses at the PET station a few days before the magnitude 7.8 Kronotskii, Kamchatka earthquake of December 5, 1997. The morphology of these sequences is illustrated in Fig. 11. Plots 1 and 2 cover 2-day intervals before the Kronotskii and Hokkaido earthquakes, respectively. While the records are generally similar, the pulse amplitudes are several

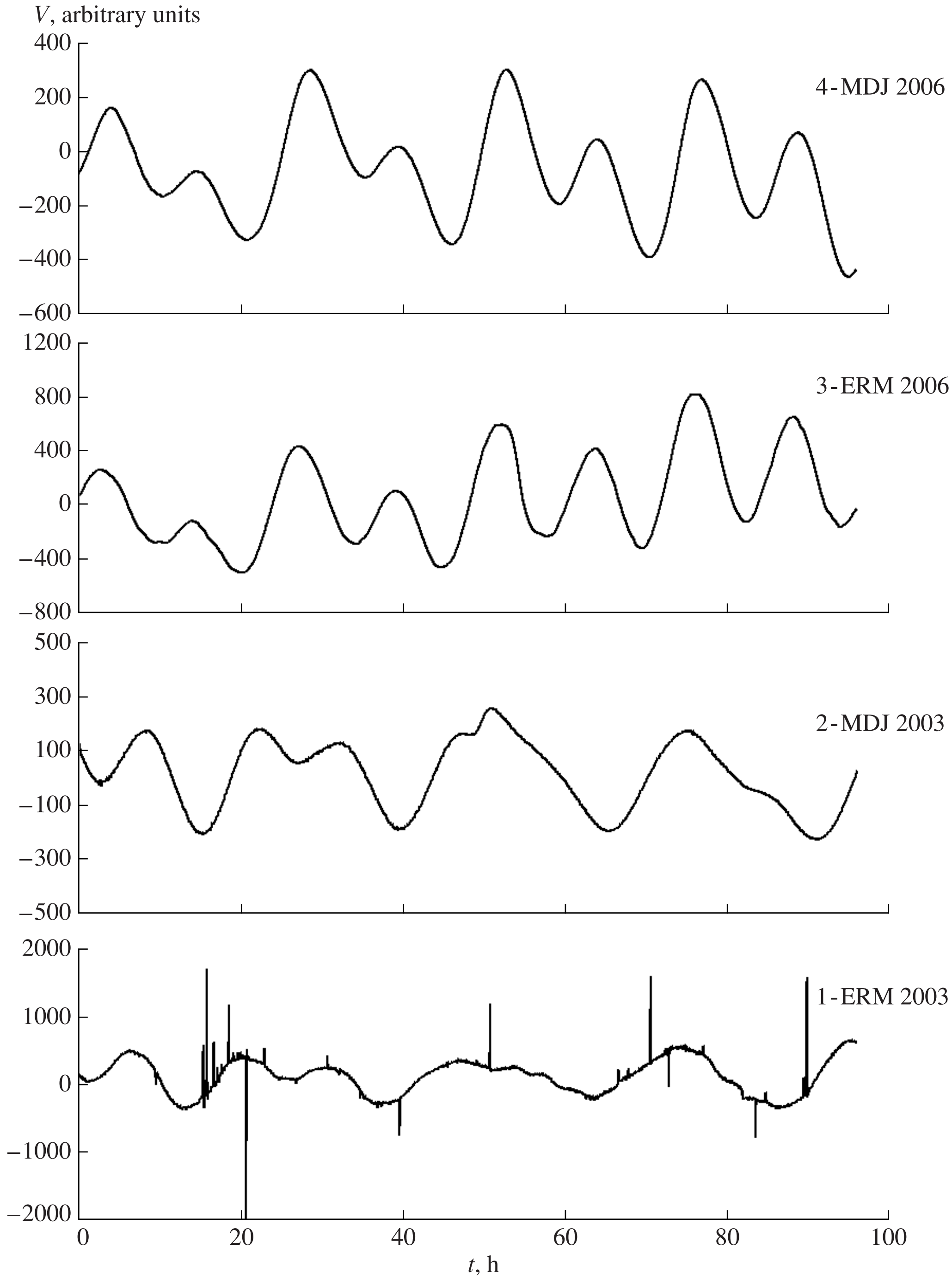

Fig. 10. Comparison of low frequency components in the records of the station ERM situated in the epicentral zone and of a distant station (MDJ) before the 2003 Hokkaido earthquake (1, 2) and after the lapse of three years following the termination of the aftershocks in 2006 (3, 4).

times greater in plot 1. This may have been due to the fact that PET was 300 km from the Kronotskii epicenter and 1750 km from the Hokkaido epicenter. However, a straightforward comparison is difficult because of the different magnitudes, 7.8 and 8.3, respectively. The analysis suggests the following: (a) the occurrence of sequences of asymmetrical pulses with periods of a few minutes before the Hokkaido earthquake is not a unique phenomenon; (b) the pulses were identified on records of the stations situated in the subduction zone; and (c) to investigate the temporal relationship between the pulses and the future earthquake we need longer observation times; this possibility, combined with the enor-

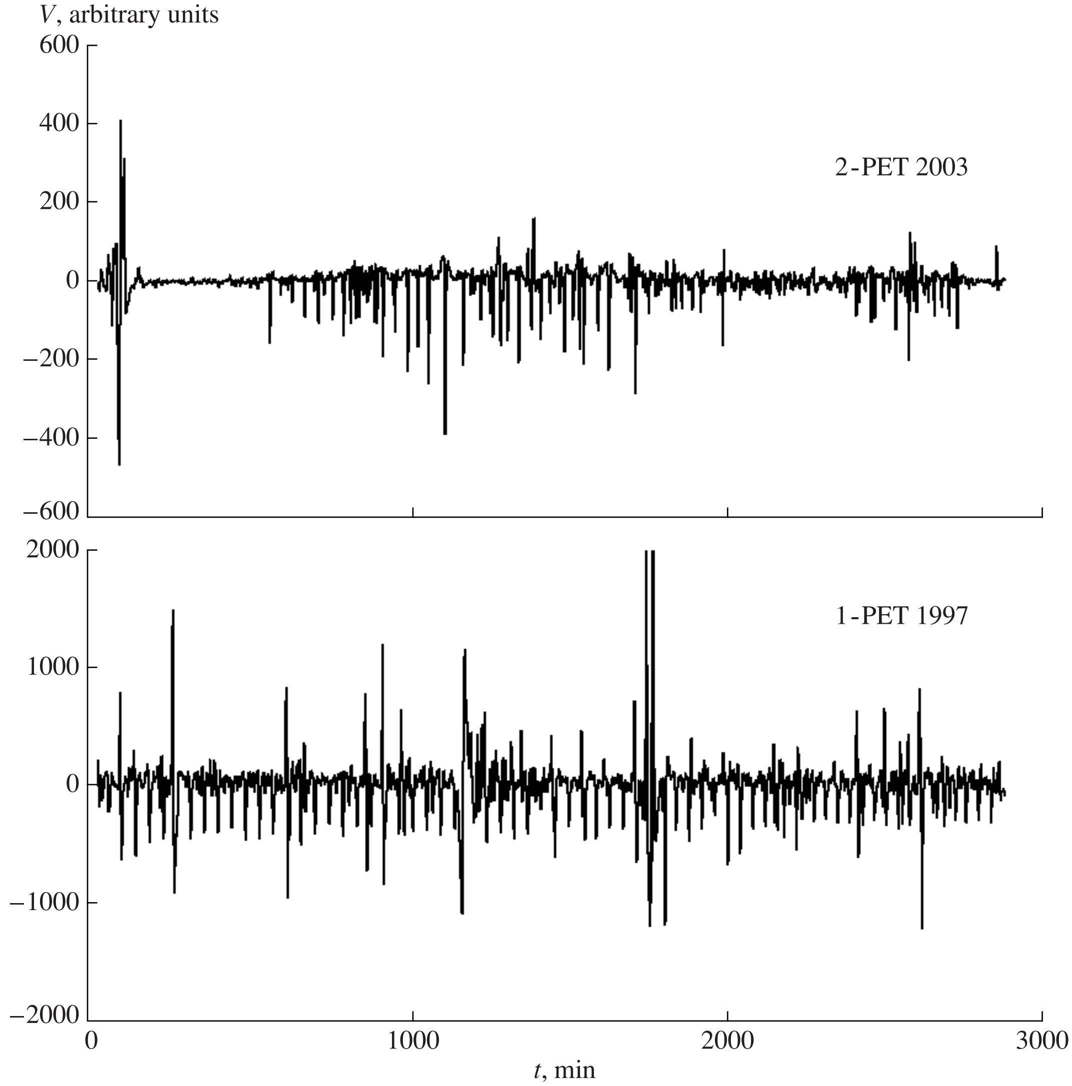

Fig. 11. Sequences of asymmetrical pulses on PET records before the 1997 Kronotskii earthquake (1) and before the 2003 Hokkaido earthquake (2).

mous amount of raw data required (tens of GB), is outside the scope of the present study.

CONCLUSIONS

(1) Stations situated in the subduction zone recorded asymmetrical microseism pulses lasting 3–10 min a few days before the magnitude 8.3 Hokkaido earthquake. No such pulses were recorded by stations outside the subduction zone. Similar pulses were also recorded before the magnitude 7.8 Kronotskii earthquake of 1997. Creeping movements are here suggested as the cause of these pulses.

(2) Synchronous pulses of microseism noise with periods of 1–3 h were recorded a few days before the Hokkaido earthquake at stations as far from the epicenter as 3100 km. The noise coherence measure was greater at stations nearer to the epicenter. What the source of this coherence was remains an open question.

(3) The above effects are similar to those arising in dissipative metastable systems; such systems seem to be parts of the Earth's lithosphere during the precursory periods of seismic disasters.

ACKNOWLEDGEMENTS

The authors are grateful to A.D. Zav'yalov for helpful remarks. This work was supported by the program "Electronic Earth" of the Russ. Acad. Sci. Presidium, by the Russian Foundation for Basic Research (grant no. 06-05-6472), by the Science Schools grant no. 5009.2006.5, and by INTAS Ref. No. 0.5-100008-7889.

REFERENCES

1. Lyubushin, A.A., Pisarenko, V.F., Ruzhich, V.V., and Buddo, V.Yu., The Identification of Periodicities in Seismic Regime, *Vulkanol. Seismol.*, 1998, no. 1, pp. 62–76.
2. Lyubushin, A.A., The Analysis of Canonical Coherences in Problems of Geophysical Monitoring, *Fizika Zemli*, 1998, no. 1, pp. 59–66.
3. Lyubushin, A.A., The Wavelet Aggregate Signal and Synchronous Spikes in Problems of Geophysical Monitoring and Earthquake Prediction, *Fizika Zemli*, 2000, no. 3, pp. 20–30.
4. Lyubushin, A.A., Periodicities and Rhythms of Global Seismicity in the 20th Century, in *Sovmestnoe zasedanie sessii nauchnogo seminara OGGGGN RAN "Teoreticheskie problemy geologii" i X nauchnogo seminara "Sistema Planeta Zemlya" po teme: "Ritmichnost' tsiklichnost' v geologii kak otrazhenie obshchikh zakonov razvitiya"* (Joint sitting of the OGGGGN RAN seminar session "Theoretical Problems of Geology" and the X seminar "The Planet Earth System", topic "Rhythmicity and Cyclicity in Geology as a Reflection of General Development Laws", February 7–8, 2002. Abstracts of papers, *OGGGGN RAN seminar*, Moscow: 2002, pp. 66–67.
5. Lyubushin, A.A., Pisarenko, V.F., Bolgov, M.V., and Rukavishnikova, T.A., A Study in the General Effects Resulting from River Drainage Variations, *Meteorol. Gidrol.*, 2003, no. 7, pp. 76–88.
6. Lyubushin, A.A. and Kopylova, G.N., Multivariate Wavelet Analysis of Electrotelluric Time Series Recorded in Kamchatka, *Fizika Zemli*, 2004, no. 2, pp. 82–96.
7. Lyubushin, A.A., Pisarenko, V.F., Bolgov, M.V., Rodkin, M.V., et al, Synchronous Variations in Caspian Sea Level as Derived from Onshore Observations, 1977–1991, *Izv. RAN. Fizika Atmosfery i Okeana*, 2004, no. 6, pp. 821–831.
8. Lyubushin, A.A. and Sobolev, G.A., Multifractal Measures of Synchronization for Microseism Oscillations with Periods of a Few Minutes, *Fizika Zemli*, 2006, no. 9, pp. 18–28.
9. Lyubushin, A.A., *Analiz dannykh sistem geofizicheskogo i ekologicheskogo monitoringa* (The Analysis of Data Acquired by Geophysical and Ecological Monitoring Systems), Moscow: Nauka, 2007.
10. Nicolis, G. and Prigogine, I., Self-organization in Nonequilibrium Systems, John Wiley and Sons, 1977.
11. Rulev, B.G., Annual Periodicity in the Emission of Microseisms and Nonuniform Rotation of the Earth, in *Zemletryaseniya i protsessy ikh podgotovki* (Earthquakes and the Precursory Processes before them), Moscow: Nauka, 1991, pp. 127–138.
12. Rykunov, L.N., Khavroshkin, O.B., and Tsyplakov, V.V., Lunar–Solar Tidal Periodicity in the Line Spectra of Time Variations of High Frequency Microseisms, *Dokl. AN SSSR*, 1980, vol. 252, no. 3, pp. 577–580.
13. Sadovskii, A.A., Introduction, in *Kompleksnye issledovaniya po fizike zemletryasenii* (Multidisciplinary Studies in Earthquake Physics), Moscow: Nauka, 1989, pp. 3–8.
14. Saltykov, V.A., Sinitsyn, V.I., and Chebrov, V.N., A Study of High Frequency Seismic Noise Based on Continuous Observations in Kamchatka, *Fizika Zemli*, 1997, no. 3, pp. 39–47.
15. Smirnov, V.B., Ponomarev, A.V., Dzhiadon, Kh., and Cherepanov, A.S., Rhythms and Deterministic Chaos in Geophysical Time Series, *Fizika Zemli*, 2005, no. 6, pp. 6–28.
16. Sobolev, G.A., The Evolution of Periodic Fluctuations of Seismic Intensity before Large Earthquakes, *Fizika Zemli*, 2003, no. 11, pp. 3–15.
17. Sobolev, G.A., Variations in Microseisms before a Large Earthquake, *Fizika Zemli*, 2004, no. 6, pp. 3–13.
18. Sobolev, G.A., Lyubushin, A.A., and Zakrzhevskaya, N.A., Synchronization of Microseism Oscillations with Periods of a Few Minutes, *Fizika Zemli*, 2005, no. 8, pp. 3–27.
19. Sobolev, G.A. and Lyubushin, A.A., Microseism Pulses as Earthquake Precursors, *Fizika Zemli*, 2006, no. 9, pp. 5–17.
20. Sobolev, G.A. and Lyubushin, A.A., Microseism Anomalies before the Sumatra Earthquake of December 26, 2004, *Fizika Zemli*, 2007, no. 5, pp. 3–16.
21. Starovoit, O.E. and Mishatkin, V.N., *Seismicheskie stantsii Rossiiskoi akademii nauk* (Seismic Stations of the Russian Academy of Sciences), Moscow–Obninsk: Geofizicheskaya sluzhba RAN, 2001.
22. Sytinskii, A.D., Recent Tectonic Movements as a Manifestation of Solar Activity, *Geomagn. Aeron.*, 1963, vol. 3, no. 1, pp. 148–156.
23. Tabulevich, V.N., *Kompleksnye issledovaniya mikroseismicheskikh kolebanii* (Comprehensive Studies of Microseism Oscillations), Nauka SO, 1986.
24. Tyupkin, Yu.S., Low-magnitude Seismicity Modulated by Tidal Strain before Large Earthquakes, *Vulkanol. Seismol.*, 2002, no. 3, pp. 3–10.
25. Bak, P., Tang, S., and Winsenfeld, K., Earthquakes as Self-Organized Phenomenon, *J. Geophys. Res.,* 1989, vol. 94, pp. 15 635–15 637.
26. Brillinger, D.R., *Time Series. Data Analysis and Theory*, New York–Chicago: Holt, Rinehart and Winston, Inc., 1975.
27. Chelidze, T. and Matcharashvili, T., Electromagnetic Control of Earthquake Dynamics?, *Computers and Geosciences*, 2003, vol. 29, pp. 587–593.
28. Cox, D.R. and Lewis, P.A.W., *The Statistical Analysis of Series of Events*, London: Methuen, 1966.
29. Currenti, G., del Negro, C., Lapenna, V., and Telesca, L., Multifractality in Local Geomagnetic Field at Etna Volcano, Sicily (Southern Italy), in *Natural Hazards and Earth System Sciences*, 2005, vol. 5, pp. 555–559.
30. Daubechies, I., *Ten Lectures on Wavelets*, No. 61 in CBMS-NSF Series in Applied Mathematics, SIAM, Philadelphia, 1992.
31. Djadkov, P.G., Induced Seismicity at the Lake Baikal: Principal Role of Load Rate, in *The 29th General Assembly of the International Association of Seismology and Physics of the Earthís Interior*, August 18–28, 1997, Abstracts of papers, Thessaloniki, Greece, p. 359.
32. Feder, J., *Fractals,* New York–London: Plenum Press, 1989.
33. Gauthier, D.J. and Bienfang, J.C., Intermittent Loss of Synchronization in Coupled Chaotic Oscillators:

Towards a New Criterion for High Quality Synchronization, *Phys. Rev. Lett.*, 1996, vol. 77, p. 1751.

34. Hardle, W., *Applied Nonparametric Regression*, Cambridge University Press, 1989.
35. Hurst, H.E., Long-term Storage Capacity of Reservoirs, *Trans. Amer. Soc. Civ. Eng.*, 1951, vol. 116, pp. 770–808.
36. Kantelhardt, J.W., Zschiegner, S.A., Konscienly-Bunde, E., et al., Multifractal Detrended Fluctuation Analysis of Nonstationary Time Series, *Physica A*, 2002, vol. 316, pp. 87–114.
37. Kobayashi, N. and Nishida, K., Continuous Excitation of Planetary Free Oscillations by Atmospheric Disturbances, *Nature*, 1998, vol. 395, pp. 357–360.
38. Mallat, S., *A Wavelet Tour of Signal Processing*, San Diego–London–Boston–New York–Sydney–Tokyo–Toronto: Academic Press, 1998.
39. Mandelbrot, B.B. and Wallis, J.R., Some Long-Term Properties of Geophysical Records, *Water Resources Res.,* 1969, vol. 5, pp. 321–340.
40. Mandelbrot, B.B., *The Fractal Geometry of Nature*, W.H. Freeman, 1983.
41. Marple, S.L., Jr., *Digital Spectral Analysis with Applications*, Englewood Cliffs, New Jersey: Prentice-Hall, Inc., 1987.
42. Nikolaev, A.V. and Nikolaev, V.A., *Earth Tides Triggering of Earthquakes,* in *Continental Earthquakes*, Beijing: Seismological Press, 1993, pp. 319–327.
43. Ott, E., *Chaos in Dynamic Systems*, Cambridge University Press, 2002.
44. Pykovsky, A., et al., *Synchronization. A Universal Concept in Nonlinear Science,* Cambridge University Press, 2003.
45. Rossler, O.E., An Equation for Continuous Chaos, *Phys. Lett.*, 1976, vol. 57, pp. 397–399.
46. Sornette, D. and Sammis, C.G., Complex Critical Exponents from Renormalization Group Theory of Earthquakes: Implications for Earthquake Prediction, *J. Phys. I. France,* 1995, vol. 5, pp. 607–619.
47. Tanimoto, T., Um, J., Nishida, K., and Kobayashi, N., Earth's Continuous Oscillations Observed on Seismically Quiet Days, *Geophys. Res. Lett.*, 1998, vol. 25, pp. 1553–1556.
48. Telesca, L., Colangelo, G., and Lapenna, V., Multifractal Variability in Geoelectrical Signals and Correlations with Seismicity: A Study Case in Southern Italy, in *Natural Hazards and Earth System Sciences*, 2005, vol. 5, pp. 673–677.
49. Wenzel, H.-G., The Nanogal Software: Earth Tide Data Processing Package ETERNA 3.30, *Marees Terrestres. Bulletin díInformations,* 1996, no. 124, pp. 9425–9439.